

Unraveling Structural Models of Graphite Fluorides by Density Functional Theory Calculations

Sang Soo Han,*^{†,‡} Ted H. Yu,[†] Boris V. Merinov,[†] Adri C. T. van Duin,[§] Rachid Yazami,[⊥] and William A. Goddard, III*,[†]

[†]Materials and Process Simulation Center (MC 139-74), California Institute of Technology, Pasadena, California 91125, [‡]Center for Materials Measurement, Korea Research Institute of Standards and Science, 209 Gajeong-Ro, Yuseong-Gu, Daejeon 305-340, Republic of Korea, [§]Department of Mechanical and Nuclear Engineering, Pennsylvania State University, University Park, Pennsylvania 16802, and

[⊥]Division of Engineering and Applied Science, California Institute of Technology, Pasadena, California 91125

Received December 14, 2009. Revised Manuscript Received January 26, 2010

Using density functional theory (DFT) calculations, we have studied structural models of graphite fluorides for five fluorine compositions; C_1F (CF_1), C_2F ($CF_{0.5}$), C_3F ($CF_{0.33}$), C_4F ($CF_{0.25}$), and $C_{16}F$ ($CF_{0.0625}$). For each composition, we considered several possible structural models and calculated heat of formation relative to the pristine graphite and F_2 molecule. We also simulated X-ray diffraction patterns for each structural model and compared those with experiments. We find, in agreement with earlier experiments, that the most stable structure of the C_1F (CF_1) has an infinite array of trans-linked cyclohexane chairs of covalent C–F bonds (1.38 Å). We also find that the effects of the layer stacking sequence such as AB or AA' is not significant. For the C_2F ($CF_{0.5}$) system, an earlier model in the literature indicated that all carbon atoms have only sp^3 hybridization due to coexistence of C–C and C–F covalent bonds. However, in this work, we propose a new C_2F ($CF_{0.5}$) crystal structure in which half of the carbon atoms has sp^3 hybridization due to C–F covalent bonds and the other half has sp^2 hybridization as found in pristine graphite. Besides, with the structural models of graphite fluorides considered in this work, their formation mechanism is also clarified. Initially, two fluorines are positioned at adjacent carbon atoms with the trans geometry, and then, one graphene layer is fully covered with fluorine while other layers are still pristine. After full coverage of the graphene layer, newly added fluorine will get located on this pristine graphene layer, and then, finally, all carbon layers are covered with fluorine leading to formation of C_1F crystal. Through this mechanism, we can explain phase transition from the C_2F to the C_1F through further fluorination, which was demonstrated by an earlier experiment.

Introduction

Graphite fluoride (CF_x or C_xF) is a fluorine-intercalated graphite compound with covalent C–F bonds.¹ Poly(carbon monofluoride) ($CF_1)_n$ and a poly(dicarbon monofluoride) ($CF_{0.5})_n$ are not only exceptional lubricants² but also excellent electrode materials^{3,4} in primary lithium batteries. The lithium primary battery using the CF_x material was first commercialized by Matsushita Electric Co. in Japan.⁵ The commercial Li/ CF_x batteries use a coke based cathode having a F/C molar ratio equal

or slightly higher than unity. These Li/ CF_1 batteries show high energy density (up to 560 W/kg), high operating voltage (2.4 V vs Li^+/Li), long shelf life (> 10 years at room temperature), stable operation, and wide operating temperatures (−40 to 170 °C).⁶ Recently, Yazami et al.⁶ reported that energy and power densities of the Li/ CF_x battery is controlled by fluorine concentration and a Li/ $CF_{0.78}$ battery shows a maximum power density of 8057 W/kg which is 14 times higher than that of the typical Li/ CF_1 battery.

Another interesting feature of CF_x materials is that C–F bonding natures depend on F concentrations. Intercalated graphites with F (CF_x , $x < 0.1$) have C–F ionic bonds, leading to an extremely high electrical conductivity of 2×10^5 S/cm.⁷ For high F concentrations such as CF_1 , the conductivities of the CF_1 compounds decrease

*To whom correspondence should be addressed. E-mail: sangsoo@kriss.re.kr (S.S.H.); wag@wag.caltech.edu (W.A.G.).

- (1) (a) Watanabe, N.; Touhara, H.; Nakajima, T.; Bartlett, N.; Mallouk, T.; Selig, H. *Inorganic Solid Fluorides*; New York, 1985; Chapter 8. (b) Watanabe, N.; Nakajima, T.; Touhara, H. *Graphite Fluorides*; Elsevier, Amsterdam, 1988.
- (2) Fusaro, R. L. *ASLE Trans.* **1975**, *20*, 15.
- (3) Watanabe, N.; Ishii, M.; Yoshizawa, S. *J. Electrochem. Soc.* **1961**, *29*, 177.
- (4) Watanabe, N.; Fukuda, M. U.S. Patent 3 536 532, **1970**, and U.S. Patent 3 700 502, **1972**.
- (5) Fukuda, M.; Iijima, T. *Power Sources* 5, Academic Press: New York, 1975, p 713.

- (6) Yazami, R.; Hamwi, A.; Guérin, K.; Ozawa, Y.; Dubois, M.; Giraudet, J.; Masin, F. *Electrochim. Commun.* **2007**, *9*, 1850.
- (7) Touhara, H.; Kadono, K.; Fujii, Y.; Watanabe, N. *Z. Anorg. Allg. Chem.* **1987**, *544*, 7.

to $\sim 10^{-14}$ S/cm due to the formation of C–F covalent bonds. For this reason, exact information regarding the crystal structures of CF_x is very important to understand and improve CF_x materials for batteries.

Several groups investigated the crystal structures of CF_x theoretically⁸ and experimentally.^{7,9} Using the X-ray powder diffraction experiment, Touhara et al.⁷ proposed a CF_1 (C_1F) structure with an infinite array of trans-linked cyclohexane chairs where the packing of corrugated layers in the CF_1 lattice is such that each carbon atom of any layers along the c axis exactly corresponds to a carbon atom in a parallel layer, meaning the covered configuration with mirror plane of symmetry, i.e., AA'/A'A type of sequence. However, Ebert et al.^{9c} proposed another CF_1 structure with cis-trans-linked cyclohexane boats from NMR second moment measurements. Charlier et al.^{8a} compared the two crystal structures of CF_1 with AAAA stacking (each carbon atom has a corresponding atom in the plane directly above and below) using density functional theory (DFT) calculation and showed that the chair conformation is more favorable by 0.145 eV per CF unit than the boat and that the transition barrier between the chair and boat conformations is 2.72 eV. Zajac et al.^{8b} investigated both chair and boat-typed CF_1 structures for AAAA, AA'/A'A, and ABAB stackings using a semiempirical quasi-relativistic INDO Hamiltonian calculation. They showed that the chair conformation is more stable than the boat conformation similar to the work by Charlier et al.;^{8a} however, the transition between these two conformations is a symmetry forbidden reaction in sharp contrast to Charlier et al.^{8a} According to the INDO calculation, various stacking sequences of CF_1 are very close on the energy scale, suggesting that in the real structure of CF_1 statistical distribution of various types of sequences can occur.

For $\text{CF}_{0.5}$ (C_2F), Kita et al.^{9e} first proposed a crystal structure based on X-ray powder diffraction (XRD) patterns. According to the model, a monolayer of C_2F contains two types of carbon atoms and a regular alternation of coupled rows of carbon atoms sp^3 -bonded to fluorine atoms (and sp^3 -bonded to each other) with

coupled rows of sp^2 -carbon atoms double-bonded to each other and forming no chemical bonds with fluorine atoms. However, this model was not able to explain the diffraction pattern peak corresponding to the parameter $c(001)$ or $c/2(002)$. Later, Touhara et al.⁷ proposed a new model in which all carbon atoms are sp^3 -hybridized. Kita et al.^{9e} experimentally reported that further fluorination into C_2F leads to C_1F . However, with the model proposed by Touhara et al.,⁷ it is not straightforward to sort out the pathway for the phase transformation from C_2F into C_1F .

Fluorination of graphite at elevated temperatures leads to the CF_1 and $\text{CF}_{0.5}$; however, fluorination at low temperatures and in the presence of catalysts results in a fluorine-graphite intercalation compound (F-GIC).¹⁰ As we already mentioned, since the F-GIC has lower fluorine concentration than CF_1 and $\text{CF}_{0.5}$, it shows good conductivity. However, it is difficult experimentally to clarify crystal structures of the F-GICs. Some research groups successively synthesized the F-GIC with stage I phases in which they reported that C–F bond length for C_xF ($2 < x < 5$) is 2.1–2.2 Å^{9f} and 1.7 Å for C_6F ,¹¹ suggesting the so-called “semi-ionic” or “semicovalent” C–F bonds. However, another experiment^{9m} on C_xF ($x = 2.47, 2.84$, and 3.61) with stage I phase by neutron diffraction shows that C–F bond length in the C_xF is essentially covalent with the bond length of 1.4 Å, and the original planar graphene sheets are buckled at the sp^3 -hybridized carbon atoms bound to fluorine atoms. In addition, DFT work^{8e} on the stage I C_3F crystal shows that the C–F bond length is 1.43–1.49 Å shorter than the previous experimentally estimated values (2.1–2.2 Å).^{9f}

In this work, we investigate crystal structures of CF_x (or C_xF) through density functional theory where we considered five different fluorine concentrations of CF_x ; CF_1 (C_1F), $\text{CF}_{0.5}$ (C_2F), $\text{CF}_{0.333}$ (C_3F), $\text{CF}_{0.25}$ (C_4F), and $\text{CF}_{0.0625}$ (C_{16}F). For each concentration, we consider several geometries and then clarify the accurate crystal structure from heat of formation results and XRD data. Together with these crystal structures, we propose a formation mechanism of graphite fluorides.

Computational Details

To investigate exact crystal structures of CF_x , we performed a series of DFT calculations in which the crystal structures with 32 carbon atoms (8 carbon atoms per layer) was fully optimized without any symmetry constraint. These works were carried out using the SeqQuest software (version 2.58a),¹² a fully self-consistent Gaussian based linear combination of atomic orbitals DFT method with double- ζ plus polarization basis sets.¹³ All calculations were based on the Perdew-Burke-Ernzerhof (PBE)¹⁴ generalized gradient approximation with pseudoatomic

- (8) (a) Charlier, J.-C.; Gonze, X.; Michenaud, J.-P. *Phys. Rev. B* **1993**, *47*, 16162. (b) Zajac, A.; Pelikán, P.; Minář, J.; Noga, J.; Straka, M.; Baňáký, P.; Biskupić, S. *J. Solid State Chem.* **2000**, *150*, 286. (c) Takagi, Y.; Kusakabe, K. *Phys. Rev. B* **2002**, *65*, 121103. (d) Pelikán, P.; Noga, J.; Biskupić, S. *J. Solid State Chem.* **2003**, *174*, 233. (e) Bettinger, H. F.; Kudin, K. N.; Scuseria, G. E. *J. Phys. Chem. A* **2004**, *108*, 3016.
- (9) (a) Rudorff, W.; Rudorff, G. Z. *Anorg. Allg. Chem.* **1947**, *293*, 281. (b) Rudorff, W. *Adv. Inorg. Chem. Radiochem.* **1959**, *1*, 223. (c) Ebert, L. B.; Brauman, J. I.; Huggins, R. A. *J. Am. Chem. Soc.* **1974**, *96*, 11. (d) Kamarchik, P.; Margrave, J. L. *Acc. Chem. Res.* **1978**, *78*, 296. (e) Kita, Y.; Watanabe, N.; Fujii, Y. *J. Am. Chem. Soc.* **1979**, *101*, 3832. (f) Mallouk, T.; Bartlett, N. *J. Chem. Soc., Chem. Commun.* **1983**, *103*. (g) Mallouk, T.; Hawkins, B. L.; Conrad, M. P.; Zilm, K.; Maciel, G. E.; Bartlett, N. *Philos. Trans. R. Soc. London, A* **1985**, *314*, 179. (h) Nakajima, T.; Molinier, M.; Motoyama, M. *Carbon* **1991**, *29*, 429. (i) Ikemiya, N.; Hara, S.; Ogino, K.; Nakajima, T. *Surf. Sci. Lett.* **1992**, *274*, L524. (j) Amine, K.; Nakajima, T. *Carbon* **1993**, *31*, 553. (k) Nakajima, T.; Tamura, T. *Synth. Met.* **1995**, *73*, 63. (l) Sato, Y.; Itoh, K.; Hagiwara, R.; Fukunaga, T.; Ito, Y. *Carbon* **2004**, *42*, 2897. (m) Sato, Y.; Itoh, K.; Hagiwara, R.; Fukunaga, T.; Ito, Y. *Carbon* **2004**, *42*, 3243. (n) Zhang, W.; Guérin, K.; Dubois, M.; Fawal, Z. E.; Ivanov, D. A.; Vidal, L.; Hamwi, A. *Carbon* **2008**, *46*, 1010.

- (10) Nakajima, T., Ed. *Fluorine-Carbon and Fluoride-Carbon Materials*; Marcel Dekker: New York, 1995.
- (11) Higiwara, R.; Lerner, M.; Bartlett, N. *J. Chem. Soc., Chem. Commun.* **1989**, 573.
- (12) Schultz, P. A. *SEQQUEST code*; Sandia National Labs: Albuquerque, NM, 2005; <http://dft.sandia.gov/Quest/>.
- (13) Mattsson, A. E.; Schultz, P. A.; Desjarlais, M. P.; Mattsson, T. R.; Leung, K. *Modell. Simul. Mater. Sci. Eng.* **2005**, *13*, R1–R31.
- (14) Perdew, J. P.; Burke, K.; Ernzerhof, M. *Phys. Rev. Lett.* **1996**, *77*, 3865.

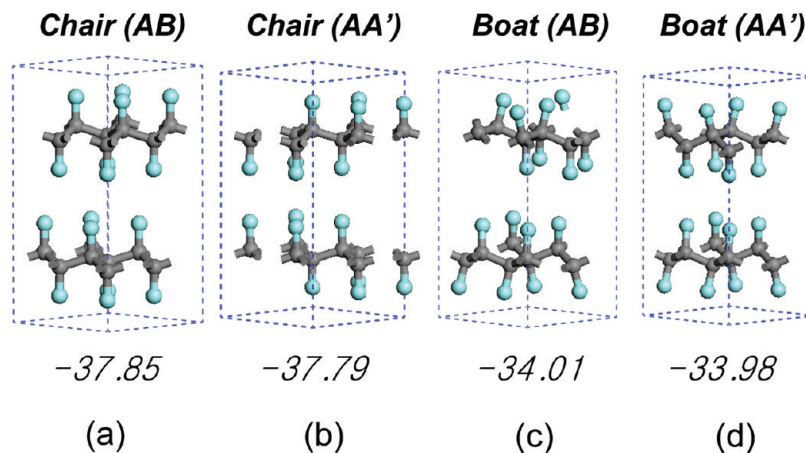


Figure 1. Structural models of C_1F (CF_1) crystal optimized by the DFT calculation where gray and cyan colors indicate carbon and fluorine atoms, respectively. Panels (a) and (b) have the infinite array of trans-linked cyclohexane chairs, while panels (c) and (d) have cis-trans-linked cyclohexane boats. Also, panels (a) and (c) have a layer stacking sequence of the AB, while panels (b) and (d) have a layer sequence of the AA'. The numbers underneath each structure show our calculated heats of formation (in kcal/mol) for the C_1F (CF_1) crystal relative to pure graphite and a F_2 molecule.

Table 1. Crystal Structures of C_1F (CF_1) Optimized by DFT with Lattice Parameters and Angles for Each Unit Cell^a

CF_1 (C_1F)	chair (AB)	chair (AA')	boat (AB)	boat (AA')
space group	$\text{P}_{3\text{M}1}$ (No. 156)	$\text{P}_{-6\text{M}2}$ (No. 187)	$\text{P}_{21/\text{C}}$ (No. 14)	P_{NNM} (No. 58)
lattice parameter (\AA)	$a = b = 2.61$ and $c = 12.39$	$a = b = 2.60$ and $c = 12.22$	$a = 12.84, b = 4.47,$ and $c = 12.57$	$a = 4.47, b = 2.58,$ and $c = 12.59$
lattice angle ($^\circ$)	$\alpha = \beta = 90$ and $\gamma = 120$	$\alpha = \beta = 90$ and $\gamma = 120$	$\alpha = \gamma = 90$ and $\beta = 168.41$	$\alpha = \beta = \gamma = 90$
density (g/cm^3)	2.82	2.88	2.84	2.84
interlayer distance (\AA)	6.19	6.11	6.29	6.30
C–F bond length (\AA)	1.38	1.38	1.38	1.38

^aThe space group is found from the optimized structures in Figure 1 using a tolerance of 0.1 \AA .

potentials and spin polarization within 3-dimensional periodic boundary conditions. The k-point sampling of $4 \times 4 \times 2$ in the Brillouin zone was carefully determined by energetic convergence. During self-consistent field (SCF) calculation, the convergence criterion of 5×10^{-4} Ry and the initial SCF blend factor of 3×10^{-1} were considered. Besides, the accelerated steepest descent method¹² for geometry optimization was used with the force convergence criterion of 5×10^{-4} Ry/bohr, and the Broyden method¹² for cell optimization was used with the stress convergence criterion of 10^{-3} GPa.

We also simulated X-ray diffraction (XRD) patterns ($5^\circ \leq 2\theta \leq 90^\circ$) for the optimized structures by DFT calculations to compare with experimental results. The simulations were performed through the commercial Cerius2 software where the Cu K α wavelength ($\lambda = 1.540562 \text{\AA}$) was used for a comparison with reported experiments.

Crystal Structures of CF_x or C_xF

CF₁ or C₁F. Figure 1 shows the four crystal structures of CF_1 considered in this work. The structures have two layers, and each layer occupy eight carbon and eight fluorine atoms. The infinite array of trans-linked cyclohexane chairs is a layered structure, derived from graphite by insertion of three covalently bonded fluorine atoms above and three fluorine atoms below every hexagon in each layer, which then becomes puckered as shown in Figure 1a,b. We also considered an infinite array of cis-trans-linked cyclohexane boats (Figure 1c,d) because the result of nuclear magnetic resonance second moment studies

supported existence of the boat-type CF_1 crystal.^{9c} However, many researchers have believed so far that the chair-type crystal structure is more plausible.^{1,8a–c,91,m} The stacking sequence of CF_1 crystal is also controversial. Currently, it is believed that the chair-type crystal with the AA' sequence (Figure 1b) is an accurate model of CF_1 .⁷

Using DFT calculations, we optimized the four crystal structures of CF_1 and calculated heat of formation relative to the pure graphite and F_2 molecule (Figure 1). The crystal structures of the optimized CF_1 are summarized in Table 1. From the heat of formation, we observe that the chair-type crystal is more stable than the boat-type as well as the AB stacking sequence is marginally favorable compared to the AA' sequence. This agrees with previous DFT calculations^{8a} on CF_1 crystals with AA stacking employing a local-density approximation, which indicated that the chair conformation is energetically favored with respect to the boat conformation by 3.34 kcal/mol (3.84 kcal/mol for the AB stacking and 3.81 kcal/mol for the AA' stacking in our work). Moreover, our calculated heat of formation at $T = 0 \text{ K}$ for the most stable chair-type CF_1 crystal with AB stacking is -37.85 kcal/mol which is very close to an experimental $T = 298 \text{ K}$ result of -39.36 kcal/mol .^{9d}

We also calculated X-ray diffraction (XRD) patterns (Figure 2) for the optimized CF_1 crystal structures in Figure 1 assuming that the X-ray source is Cu K α for comparison with experiments. Overall, all XRDs for the

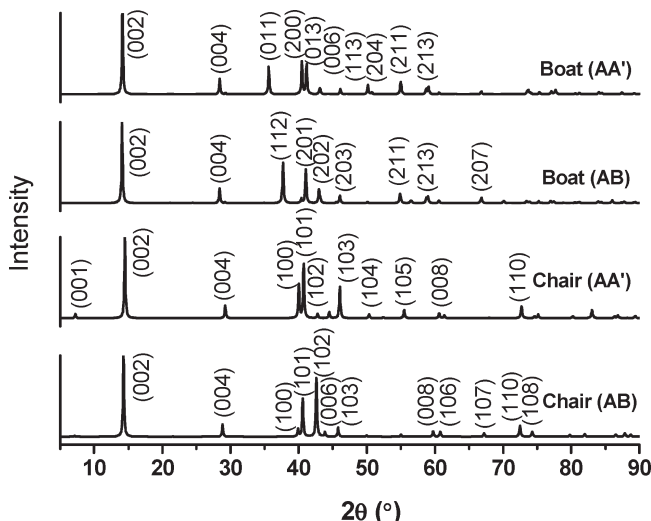


Figure 2. Simulated XRD patterns using the Cu K α wavelength for the C₁F (CF₁) crystal structures shown in Figure 1.

four crystals are similar; however, we can distinguish between chair and boat-type structures from one peak ((112) for the boat with the AB stacking and (011) for the boat with the AA' stacking) in the range of 35–40° and another peak near 72° (corresponding to (110) in the chair-type CF₁). Also, we can distinguish the chair-type CF₁ with the AB or AA' stacking from one very weak peak near 7°. Two experimental XRDs for CF₁ crystal reported in 1979^{9e} and 2004^{9f} show similar patterns, and we find that these results agree best with our XRDs for chair-typed models due to the absence of a peak near 35–40° and the presence of the (110) peak. The two experiments did not show a peak near 7°, leading to the chair-type CF₁ with the AB stacking. However, we cannot ignore the possibility that it is not shown because of very weak intensity.

CF_{0.5} or C₂F. Figure 3 shows seven candidates for the C₂F crystal structures (C: 32 and F: 16) with four carbon layers. The information of the optimized crystal structures is summarized in Table 2. In Figure 3, all carbon atoms in the first five structural models (Figure 3a–e) have only sp³ bonding character, while both sp² and sp³ carbon bonding characters are found in the last two models (Figure 3f,g). Kita et al.^{9e} first proposed the C₂F crystal structure of a monoclinic model from XRD analysis which is similar to Figure 3g; the difference is shown in Figure S2 in the Supporting Information. Later, Touhara et al.⁷ also reported a XRD result similar to one of Kita et al.;^{9e} however, they claimed that the XRD should be for a hexagonal structure not a monoclinic. Thus, we also consider the model of Touhara et al.⁷ which is Figure 3e.

According to heat of formation values seen in Figure 3, the structural models of Figure 3d,e are most favorable, supporting the Touhara et al.'s model.⁷ We find that the effect of the layer sequence in the C₂F system is not significant, as like the C₁F case. Furthermore, our DFT calculation predicts that C–F bond length in the C₂F system is 1.38 Å, except the case of Figure 3g with 1.41 Å.

The value (1.38 Å) is the same as that of the C₁F system. When a carbon layer is partially covalently bonded to fluorine atoms, the C–F bond length is slightly longer than when one is fully occupied by fluorine, as shown in Figure 3g.

To clarify the C₂F crystal structure, we also simulated XRD patterns (Figure 4) for the seven models shown in Figure 3 and then compared them with two experimental results (Kita et al.^{9e} and Touhara et al.⁷). According to the XRD experiment performed by Kita et al.,^{9e} high crystalline C₂F shows three peaks at 10.1°, 20.1°, and 41.8° in the 2θ range of 5–50° where the C₂F sample was synthesized by fluorination reaction of graphite with particle sizes of 200–250 mesh at 370 °C for 132 h and then followed by additional fluorination at 600 °C for 120 h. Compared with our simulated XRDs, the structural model of Figure 3g proposed by Kita et al.^{9e} does not match well with the experimental result. The most possible candidate is Figure 3d or e which is energetically favorable. However, Kita et al.^{9e} also reported a XRD pattern for another C₂F sample which was synthesized by fluorination reaction of graphite with particle size of 20–50 mesh at 375 °C for 180 h where 9.8°, 20.1°, 31.2°, and 45.8° in the 2θ range of 5–50°. Through a comparison of this experiment and our simulation, the structure in Figure 3f is also a possible crystal structure due to the third peak near 30° where the Figure 3d,e does not show the peak. The XRD experiment performed by Touhara et al.⁷ is similar to the second result of the Kita et al.^{9e} (using graphite of 20–50 mesh) in that it also shows the third peak near 30°, supporting the structure in Figure 3f. Moreover, an NMR¹⁵ and an XPS¹⁶ study on the C₂F crystal shows that carbon atoms in sp² as well as sp³ hybridization remain in the crystal, which further supports the structure in Figure 3f as the crystal structure of C₂F. While our calculations indicate that structure in Figure 3f is less stable than that in Figure 3d,e, this energy difference is not very substantial, so entropic contributions could certainly cancel out this energy difference at room-temperature conditions.

Kita et al.^{9e} also investigated the variation for XRD patterns of graphite fluorides with the reaction time for the fluorination of graphite and showed that the fluorination first leads to the formation of C₂F, but further fluorination leads subsequently to the formation of C₁F. To explain this phenomenon, we added a fluorine molecule or two fluorine atoms into the C₂F crystal of Figure 3d and then performed a geometry optimization process using the DFT calculation. The optimized structures are shown in Figure S3 in the Supporting Information. Although the further fluorination into the structural model of Figure 3d proceeds, the newly added fluorine molecule and atoms do not react with carbon atoms but stay between carbon layers, indicating that there is no C–C bond breaking. Thus, with the model of Figure 3d,

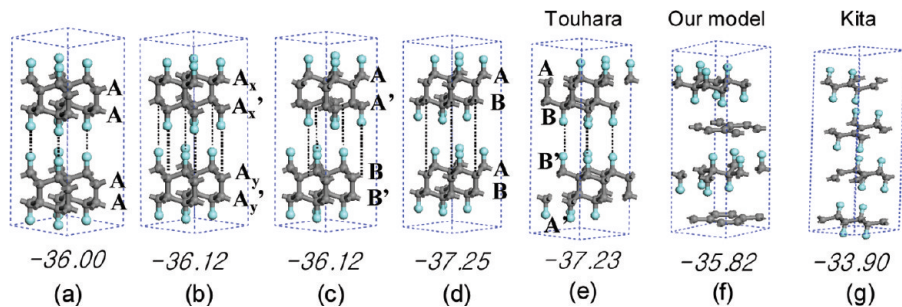


Figure 3. Structural models of C_2F ($CF_{0.5}$) crystal optimized by the DFT calculation where gray and cyan colors indicate carbon and fluorine atoms, respectively. The first five models have only the sp^3 hybridized carbon atoms in the stage II, while the last two models have both sp^2 and sp^3 carbon atoms in the stage I. Panel (e) is similar to a model proposed by Touhara et al.,⁷ and panel (g) is similar to a model by Kita et al.^{9c} The numbers underneath each structure show the heats of formation (in kcal/mol) of the C_2F ($CF_{0.5}$) crystal relative to a pure graphite and a F_2 molecule, and the detailed atomic configurations of carbon and fluorine atoms in panels (a)–(e) are shown in the Supporting Information (Figure S1).

Table 2. Crystal Structures of C_2F ($CF_{0.5}$) Optimized by DFT Where Lattice Parameters and Angles Are for Each Unit Cell^a

$\text{CF}_{0.5}(\text{C}_2\text{F})$	(a)	(b)	(c)	(d)
space group	P_{-6M2} (No. 187)	$P_{63/\text{MMC}}$ (No. 194)	$P_{63/\text{MMC}}$ (No. 194)	P_{-3M1} (No. 164)
lattice parameter (Å)	$a = b = 2.56$ and $c = 7.95$	$a = b = 2.59$ and $c = 15.84$	$a = b = 2.56$ and $c = 15.84$	$a = b = 2.56$ and $c = 8.59$
lattice angle ($^\circ$)	$\alpha = \beta = 90$ and $\gamma = 120$	$\alpha = \beta = 90$ and $\gamma = 120$	$\alpha = \beta = 90$ and $\gamma = 120$	$\alpha = \beta = 90$ and $\gamma = 120$
density (g/cm ³)	3.17	3.18	3.46	2.93
interlayer distance (Å)	7.95	7.92	7.92	8.59
C–F bond length (Å)	1.38	1.38	1.38	1.38

$\text{CF}_{0.5}(\text{C}_2\text{F})$	(e)	(f)	(g)
space group	P_{-3M1} (No. 164)	P_1 (No. 1)	$P_{21/\text{M}}$ (No. 11)
lattice parameter (Å)	$a = b = 2.56$ and $c = 17.18$	$a = b = 2.53$ and $c = 18.61$	$a = 21.48, b = 2.55$, and $c = 4.13$
lattice angle ($^\circ$)	$\alpha = \beta = 90$ and $\gamma = 120$	$\alpha = \beta = 90$ and $\gamma = 120$	$\alpha = \gamma = 90$ and $\beta = 94.87$
density (g/cm ³)	2.92	2.78	2.54
interlayer distance (Å)	8.59	4.66	5.35
C–F bond length (Å)	1.38	1.38	1.41

^aThe space group is found from the optimized structures in Figure 3 using the tolerance of 0.1 Å.

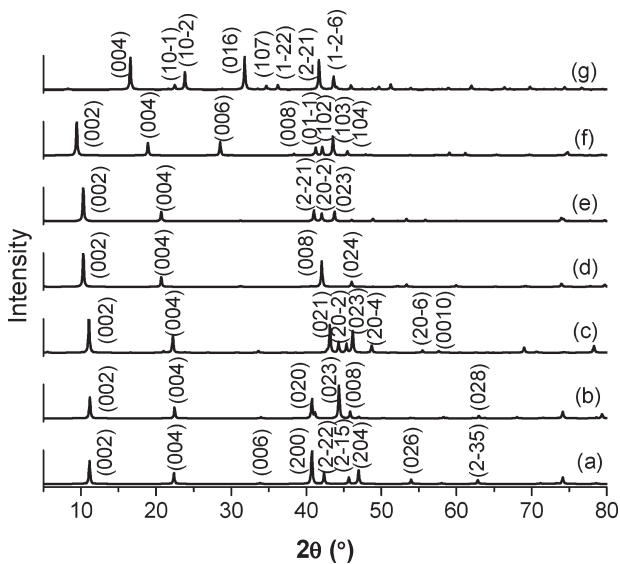


Figure 4. Simulated XRD patterns using the Cu K α wavelength for the C₂F (CF_{0.5}) crystal structures shown in Figure 3.

one is not able to explain the experimental phase transformation from C_2F into C_1F . However, we are able to explain this phenomenon with the model of Figure 3f. The details of these simulations will be discussed in Formation Mechanism of Graphite Fluorides.

CF_{0.33} or **C₃F**. Mallouk and Bartlett^{9f} first proposed a structural model of the C₃F where they used the concept of a planar structure of fluorographite matrixes and the notation of the semi-ionic C–F bond (2.1–2.2 Å) but completely rejected the presence of sp³ carbon. Bettinger et al.^{8e} performed DFT calculations to investigate crystal structures of the C₃F compound where they considered two different fluorine arrangements called “ortho” and “meta”. However, the calculations showed that the compound has a structure with nonplanar arrangement of carbon atoms and a significantly shorter C–F bond (1.43–1.49 Å) than the previous one (2.1–2.2 Å).

Figure 5 shows the stage I C_3F crystal structures (C: 36 and F: 12) with two graphene layers considered in this work, and the detailed information for crystal structures is summarized in Table 3. The “ortho” (Figure 5a,b) and “meta” (Figure 5c,d) structures are from Bettinger et al.^{8e} where the “ortho” means that the fluorine atoms on opposing sides of a graphite sheet are bonded to neighboring carbon atoms, while in the “meta” the fluorine atoms are bonded to second-nearest neighboring carbon atoms. We also investigated another C_3F crystal structure (Figure 5e) where one graphene sheet is not fluorinated, but another is partially fluorinated with trans-linked cyclohexane chairs.

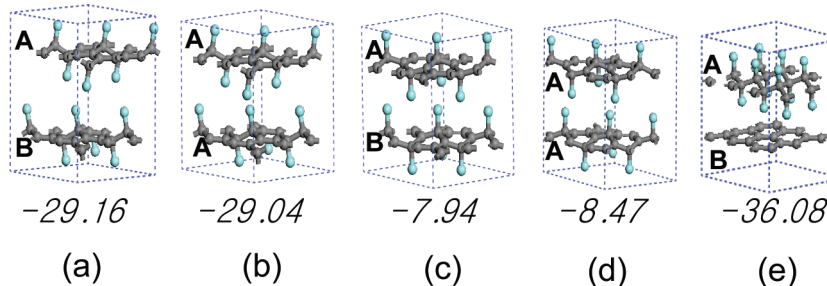


Figure 5. Structural models of the stage I C_3F ($\text{CF}_{0.33}$) crystal optimized by our DFT calculations where gray and cyan colors indicate carbon and fluorine atoms, respectively. Arrangements of fluorine atoms can be characterized by their relative orientation on opposing sides of the sheet, “ortho” for panels (a) and (b), and “meta” for panels (c) and (d). Note that the “para” orientation is identical to the “ortho”. In the first four models, fluorine is positioned on every carbon layer, while in the last model there is a pristine graphene layer. The numbers underneath each structure are our calculated heats of formation (in kcal/mol) of the C_3F ($\text{CF}_{0.33}$) crystal relative to a pure graphite and a F_2 molecule.

Table 3. Crystal Structures of C_3F ($\text{CF}_{0.33}$) Optimized by DFT Where Lattice Parameters and Angles Are for Each Unit Cell^a

$\text{CF}_{0.33}$ (C_3F)	(a)	(b)	(c)	(d)	(e)
space group	P_{21} (No. 4)	C_{2221} (No. 20)	$\text{P}_{-3}\text{C}1$ (No. 165)	C_{2}/C (No. 5)	C_M (No. 8)
lattice parameter (Å)	$a = 4.30, b = 11.15,$ and $c = 4.28$	$a = 7.44, b = 4.29,$ and $c = 10.11$	$a = b = 4.28$ and $c = 10.09$	$a = 7.40, b = 4.27,$ and $c = 13.80$	$a = 12.89, b = 2.50,$ and $c = 17.30$
lattice angle (°)	$\alpha = \gamma = 90$ and $\beta = 60.22$	$\alpha = \beta = \gamma = 90$	$\alpha = \gamma = 90$ and $\beta = 131.36$	$\alpha = \gamma = 90$ and $\beta = 122.45$	$\alpha = \gamma = 90$ and $\beta = 135.14$
density (g/cm ³)	2.05	2.26	2.28	1.98	1.93
interlayer distance (Å)	5.58	5.06	5.05	5.82	5.88
C–F bond length (Å)	1.43	1.44	1.53	1.51	1.40

^aThe space group is found from the optimized structures in Figure 5 using the tolerance of 0.1 Å.

Similar to C_1F and C_2F systems, the layer stacking sequence is not significant in the C_3F case and the “ortho” structure is more stable than the “meta” which agrees with Bettinger et al.^{8e} However, we find that the most favorable structure is Figure 5e with heat of formation of -36.08 kcal/mol, leading to the suggestion that pristine graphene layers can be found at the composition of C_3F . The C–F bond length for the structure in Figure 5e is 1.40 Å lower than those (1.43–1.53 Å) in the “ortho” and “meta” structures but longer than that reported in the previous sections (1.38 Å) for C_1F and C_2F .

Our proposed structure in Figure 5e is in good agreement with neutron diffraction experiments^{9m} for C_xF ($x = 2.47, 2.84$, and 3.61) showing that the C–F bond nature is covalent and the original planar graphene sheets are buckled at the sp^3 hybridized carbon atoms bound to fluorine atoms and that a network of the conjugated bonds is maintained between the carbon atoms not bound to fluorine atoms. On the basis of this fact, the authors proposed a structure model similar to our Figure 5e where the experimental C–F bond length of 1.40 Å is exactly same to our calculated value.

Figure 6 shows XRD patterns for the five C_3F crystals in Figure 5 where only the Figure 5e structure (which is energetically the most stable) has the (001) peak. Experimental XRD for the stage I $\text{C}_{2.9}\text{F}$ system^{9h} shows four peaks, (001) at 7.8° , (002) at 15.5° , (003) at 23.5° , and (004) at 31.0° in the range of 2θ from 5° to 50° , which is in good agreement with our simulation results, which show peaks (001) at 7.5° , (002) at 15.1° , (003) at 22.7° , and (004) at 30.4° . Furthermore, we found an interlayer distance in

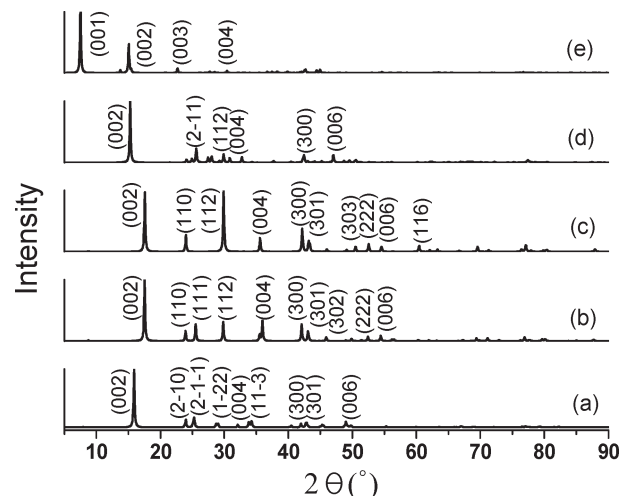


Figure 6. Simulated XRD patterns using the $\text{Cu K}\alpha$ wavelength for the C_3F ($\text{CF}_{0.33}$) crystal structures shown in Figure 5.

the simulated C_3F structure (Figure 5e) of 5.88 Å, similar to the experimental value of 5.71 Å.

$\text{CF}_{0.25}$ or C_4F . The C_4F was first synthesized by Rudorff and Rudorff in 1947 by fluorination of graphite using a mixture of F_2 and gaseous HF at room temperature.^{9a} After then, several structural models of the C_4F compound have been proposed.¹⁷ The first model that was suggested is a hexagonal structure that displays complete planarity in the C_4F monolayers and has semi-ionic C–F bonds where the vertical C–F bonds are at an angle of 90° to the plane and three C–C bonds are at an

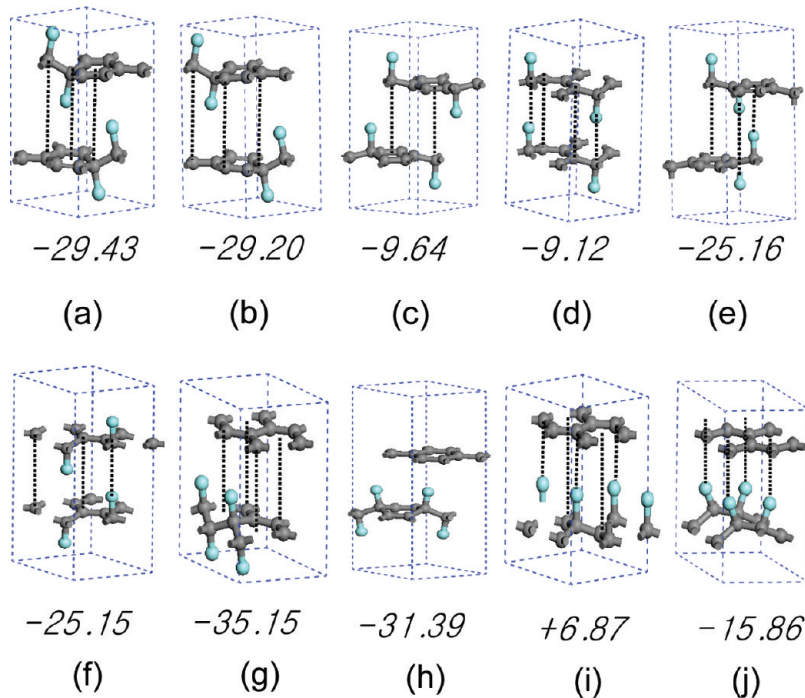


Figure 7. Structural models of C_4F ($\text{CF}_{0.25}$) crystal optimized by the DFT calculation where gray and cyan colors indicate carbon and fluorine atoms, respectively. In panels (a–f), fluorine atoms are positioned on both graphene layers, while in panels (g–j) they are on only one layer. The fluorine atoms have “ortho” arrangement in panels (a) and (b), “meta” in panels (c) and (d), and “para” in panels (e) and (f). The graphene layers in panels (a), (c), (e), (g), (h), (i), and (j) have an AB stacking sequence, while the AA stacking is in panels (b), (d), and (f). The numbers underneath each structure shows our calculated heats of formation (in kcal/mol) relative to pure graphite and F_2 molecule.

angle of 120° .^{9a} However, later the model was contradicted by the NMR experiment¹⁸ indicating that the spectra of the C_4F compound lie in the range of the chemical shifts of graphite sp^2 carbon and $\text{C}-\text{F}$ bond sp^3 carbon. Moreover, Mitkin¹⁷ proposed a model of the C_4F which has regular distorted regions of the graphite sp^2 plane with three $\text{C}-\text{C}$ sp^3 bonds and one covalent $\text{C}-\text{F}$ sp^3 bond, as well as structurally isolated regular hexagonal regions of conjugation of three $\text{C}-\text{C}$ bonds. The Mitkin’s model is shown in Figure 7e,f (note that there is no mention about a stacking sequence of graphene layers in his model).

In this work, we considered ten crystal structures (C: 16, F: 4) with two graphene layers shown in Figure 7 where the stage I (Figure 7a,h) and stage II (Figure 7i,j) structures are considered. In stage I compounds, the fluorine is located between each carbon layers to yield CFCF layers stacking, while in stage II it occupies every other layer with a stacking sequence of CCFCCF .¹⁹ From heat of formation results, we find that the stage I structure is generally more favorable than the stage II, and the layer sequence effect on the C_4F crystals is not significant although structures with the AB stacking have slightly higher heat of formation than ones with the AA stacking (e.g., -29.43 kcal/mol vs -29.20 for the “ortho” structure, -9.64 vs -9.12 for the “meta”, and -25.16 vs -25.15 for the “para”). Among the “ortho”, “meta”, and “para” structures, the stability order is “ortho” >

“para” > “meta”. According to our DFT calculations, the most favorable structure is Figure 7g with heat of formation of -35.15 kcal/mol where all fluorine atoms are positioned on the same layer have covalent $\text{C}-\text{F}$ bonds (1.41 Å in Table 4) along adjacent carbon atoms with “ortho” geometry. We find that the model shown in Figure 7g is more favorable than the Mitkin’s model in Figure 7e,f. Like the Mitkin’s model, our structural model is able to explain the experimental evidence on coexistence of sp^2 and sp^3 $\text{C}-\text{C}$ bonds and sp^3 $\text{C}-\text{F}$ bonds.

In Figure 8, we show simulated XRDs for the ten C_4F crystal structures of Figure 7, in which we can compare with the experimental results for the stage I $\text{C}_{3.9}\text{F}$ compound.^{9h} The experimental XRD is similar to our calculation XRD for our most favorable structure in Figure 7g. In the experiment, all of (001), (002), (003), and (004) peaks were observed. Among them, the (002) peak is strongest and the other diffraction peaks are weak, which is in good agreement with our calculation. The experimental c -axis value of the C_4F compound is 10.55 Å which is significantly higher than our calculated result (9.44 Å). From these experimental XRD results, Nakajima et al.^{9h} proposed a structure model similar to Mitkin’s suggestions (Figure 7e or f).¹⁷ According to our calculated XRDs for the structures of Figure 7e,f, the (001) peak found below 10° is strongest, which is different from the experiment. Therefore, we believe that the most plausible crystal structure of the C_4F is the Figure 7g predicted by our DFT calculation, rather than the Mitkin’s model.¹⁷

$\text{CF}_{0.0625}$ or C_{16}F . For this composition, nine structure candidates (C: 32, F: 2) seen in Figure 9 are considered

(18) Wilkie, C. A.; Kin, G.-Y.; Haworth, D. T. *J. Solid State Chem.* 1979, 30, 197.

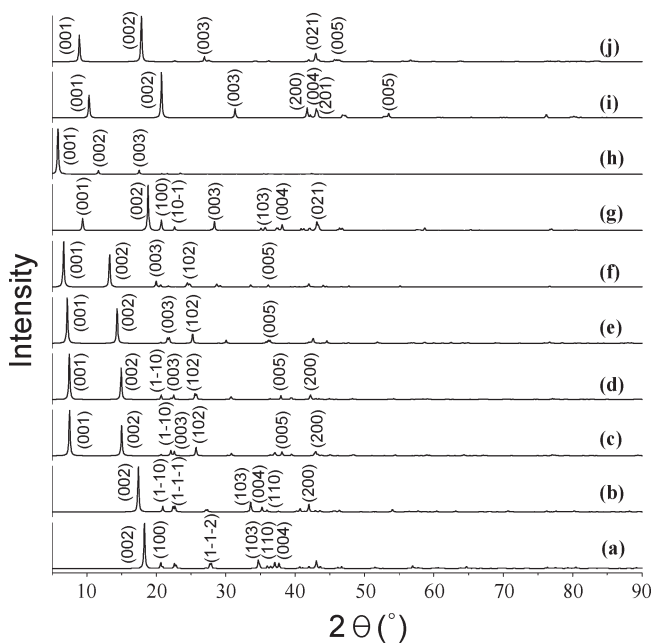
(19) Lam, P.; Yazami, R. *J. Power Sources* 2006, 153, 354.

Table 4. Crystal Structures of C_4F ($\text{CF}_{0.25}$) Optimized by DFT (shown in Figure 7) Where Lattice Parameters and Angles Are for Each Unit Cell^a

$\text{CF}_{0.25}$ (C_4F)	(a)	(b)	(c)	(d)	(e)
space group	$\text{C}_{\text{MC}21}$ (No. 36)	C_{2221} (No. 20)	$\text{C}_{2/\text{M}}$ (No. 12)	P_C (No. 7)	$\text{P}_{3\text{M}1}$ (No. 156)
lattice parameter (Å)	$a = 4.99, b = 8.49,$ and $c = 9.70$	$a = 4.99, b = 8.48,$ and $c = 10.19$	$a = 8.56, b = 4.94,$ and $c = 11.80$	$a = c = 4.95$ and $b = 11.85$	$a = b = 4.97$ and $c = 12.34$
lattice angle (°)	$\alpha = \beta = \gamma = 90$	$\alpha = \beta = \gamma = 90$	$\alpha = \beta = \gamma = 90$	$\alpha = \gamma = 90$ and $\beta = 60$	$\alpha = \beta = 90$ and $\gamma = 120$
density (g/cm ³)	2.16	2.06	1.78	1.77	1.69
interlayer distance (Å)	4.85	5.10	5.90	5.90	6.17
C–F bond length (Å)	1.45	1.45	1.53	1.52	1.48

$\text{CF}_{0.25}$ (C_4F)	(f)	(g)	(h)	(i)	(j)
space group	C_M (No. 8)	P_M (No. 6)	$\text{C}_{\text{MM}2}$ (No. 35)	$\text{P}_{3\text{M}1}$ (No. 156)	$\text{P}_{\text{MA}2}$ (No. 28)
lattice parameter (Å)	$a = 8.61, b = 4.97,$ and $c = 13.34$	$a = 4.29, b = 2.48,$ and $c = 9.44$	$a = 8.58, b = 4.96,$ and $c = 15.18$	$a = 5.00, b = 5.00,$ and $c = 8.56$	$a = 2.48, b = 4.29,$ and $c = 9.93$
lattice angle (°)	$\alpha = \beta = \gamma = 90$	$\alpha = \beta = \gamma = 90$	$\alpha = \beta = \gamma = 90$	$\alpha = \beta = 90$ and $\gamma = 120$	$\alpha = \beta = \gamma = 90$
density (g/cm ³)	1.56	2.22	1.38	2.40	2.11
interlayer distance (Å)	6.17	4.72	5.90	5.90	6.30
C–F bond length (Å)	1.48	1.41	1.49	1.49	1.42

^aThe space group is found from the optimized structures in Figure 7 using the tolerance of 0.1 Å.



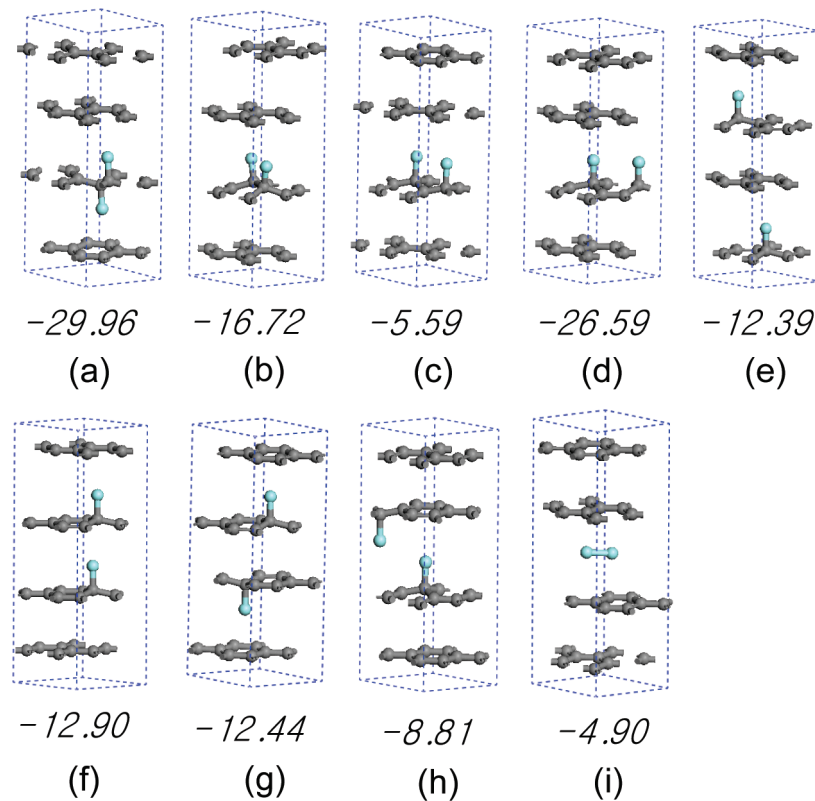


Figure 9. Structural models of C_{16}F ($\text{CF}_{0.0625}$) crystal optimized by the DFT calculation where gray and cyan colors indicate carbon and fluorine atoms, respectively. Two fluorine atoms in panels (a) and (b) located on carbon atoms with the “ortho” geometry, while with the “meta” geometry in panel (c) and with the “para” geometry in panel (d). Panels (a) and (f) are a mixture of the stage I and III. Panels (b), (c), (d), (h), and (i) are in the stage IV, and panels (e) and (g) are in the stage II. The numbers underneath each structure reflect our calculated heats of formation (in kcal/mol) of the C_{16}F ($\text{CF}_{0.0625}$) crystal relative to a pure graphite and a F_2 molecule.

Table 5. Crystal Structures of $\text{CF}_{0.0625}$ (C_{16}F) Optimized by DFT (shown in Figure 9) Where Lattice Parameters and Angles Are for Each Unit Cell^a

$\text{CF}_{0.0625}$ (C_{16}F)	(a)	(b)	(c)	(d)	(e)
space group	C_2 (No. 5)	C_M (No. 8)	P_M (No. 6)	$\text{P}_{3\text{M}1}$ (No. 156)	C_M (No. 8)
lattice parameter (\AA)	$a = 8.53, b = 4.93,$ and $c = 18.54$	$a = 8.54, b = 4.93,$ and $c = 18.79$	$a = 16.06, b = 2.47,$ and $c = 4.28$	$a = b = 4.93$ and $c = 15.77$	$a = 8.55, b = 4.94,$ and $c = 19.24$
lattice angle ($^\circ$)	$\alpha = \gamma = 90$ and $\beta = 117.40$	$\alpha = \gamma = 90$ and $\beta = 117.03$	$\alpha = \beta = \gamma = 90$	$\alpha = \beta = 90$ and $\gamma = 60$	$\alpha = \gamma = 90$ and $\beta = 116.23$
density (g/cm^3)	2.02	1.99	2.07	2.11	1.93
interlayer distance (\AA)	4.64	5.97	5.29	5.00	5.04
C–F bond length (\AA)	1.47	1.46	1.53	1.46	1.53
$\text{CF}_{0.0625}$ (C_{16}F)	(f)	(g)	(h)	(i)	
space group	C_M (No. 8)	$\text{C}_{2/\text{M}}$ (No. 12)	C_M (No. 8)	P_1 (No. 1)	
lattice parameter (\AA)	$a = 8.55, b = 4.94,$ and $c = 18.87$	$a = 8.55, b = 4.94,$ and $c = 18.87$	$a = 8.55, b = 4.94,$ and $c = 17.33$	$a = b = 4.93$ and $c = 17.24$	
lattice angle ($^\circ$)	$\alpha = \gamma = 90$ and $\beta = 116.95$	$\alpha = \gamma = 90$ and $\beta = 116.93$	$\alpha = \gamma = 90$ and $\beta = 119.54$	$\alpha = 91.04, \beta = 89.51,$ and $\gamma = 120.01$	
density (g/cm^3)	1.98	1.98	2.21	1.94	
interlayer distance (\AA)	4.82	4.82	4.31	5.90	
C–F bond length (\AA)	1.56	1.56	1.55		

^a Here, the space group is found from the optimized structures in Figure 9 using the tolerance of 0.1 \AA .

carbon layer to previous C–F bonds, is the most favorable. After adding two additional fluorine atoms to the structure in Figure 11b, we find that the most plausible structure is Figure 11e where one carbon layer is fully covered by fluorine while others are pristine (a mixture of the stage I and III). Putting two more fluorine atoms into the Figure 11e, we consider two possible cases where the added

fluorine locates on the first carbon layer (Figure 11f) and on the second layer (Figure 11g). Energetically, these two structures show the same structure stability, indicating that both options are equally likely to be observed. The finding of the structure depends on statistical distribution, which will be reported in detail later (Twelve-Layer Calculations with the Dreiding-Force Field). Further fluorination of the

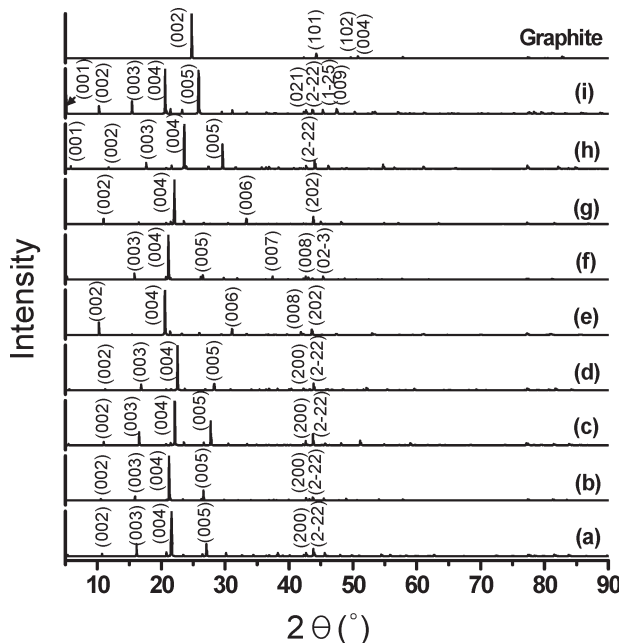


Figure 10. Simulated XRD patterns using the Cu K α wavelength for the C₁₆F (CF_{0.0625}) crystal structures shown in Figure 7.

Figure 11f,g leads to two possible C₂F crystals (Figure 11h,i) where two carbon layers are fully covered with fluorine while others are pristine graphene layers. The structure in Figure 11h is exactly the same as that in Figure 3f, which indicates that there exists a low-energy fluorination pathway for the formation of this structure. However, we cannot explain other C₂F crystal structures, proposed by Kita et al.^{9e} and Touhara et al.⁷ (see Figure 3 and the section CF_{0.5} or C₂F) through this mechanism.

Starting from the structures in Figure 11h–g, we can follow the phase transition from C₂F crystal into C₁F crystal caused by further fluorination. According to this formation mechanism, we find the C_{1.33}F (or CF_{0.75}) crystal (Figure 11p) during the phase transition where three carbon layers show full coverage with fluorine and one layer is pristine, and there exists both sp² and sp³ carbon hybridization in all graphite fluorides except in the C₁F crystal (Figure 11q). If we start the C₂F fluorination with the crystal structure proposed by Touhara et al. (Figure 3d) by adding a fluorine molecule or two fluorine atoms into this structure, we find that the newly added fluorine molecule or fluorine atom does not react with carbon atoms and stays between carbon layers (Figure S3 in the Supporting Information), indicating that there is no C–C bond breaking where our DFT calculation shows the C–C binding energy of 90 kcal/mol (Figure S4 in the Supporting Information). Thus, with the model⁷ of C₂F, one cannot explain the experimental phase transformation from C₂F into C₁F. Accordingly, in room temperature synthesis (fluorine source: F atoms), the Touhara et al.’s structure (Figure 3e) would not be found. Instead, our model (Figure 3f) suggested in this work would be observed.

Figure 12 shows the formation mechanism of graphite fluorides when the fluorination source is F₂ molecules.

A F₂ molecule can thermodynamically intercalate between two graphene layers (Figure 12a), and the graphite fluoride of C₁₆F like Figure 12b can be formed. Further fluorination by two more F₂ leads to C₈F structures such as Figure 12c or d where it is noticeable that in Figure 12c C–C bonds between two carbon layers starts to form although Figure 12d is thermodynamically most favorable at this composition. In the case of C₄F composition, Figure 12g with C–C bonds is energetically slightly more stable than Figure 12h. Further fluorination of Figure 12g,h leads to Figure 12j,k with a composition of C₂F, respectively, in which the Figure 12j is the same as a model suggested by Touhara et al.⁷ and the Figure 12k is our model suggested in this work. As already explained, the Figure 12j is not able to transform another structure by further fluorination (Figure S3 in the Supporting Information). However, our model of Figure 12k is possible by following Figure 12n (C_{1.33}F composition) and Figure 12o (C₁F composition) where the formed C₁F structure (Figure 12o) is of chair-type. According to this mechanism, direct fluorination of F₂ energetically prefer the formation of Figure 12j suggested by Touhara et al.⁷ however, our model (Figure 12o) can be also found. Besides, with our model, one can explain the phase transformation of C₂F into C₁F by further fluorination of F₂ gases, which was experimentally observed.^{9e}

In Figure 12, we assumed that F₂ molecules would dissociate and form C–F bonds with “meta” configuration. We also consider formation mechanisms of graphite fluoride by “ortho” and “para” configurations shown in Figure S5 in the Supporting Information. In the mechanism by the “ortho” configuration (Figure S5A in the Supporting Information), the final product is a structure of C₈F in which all fluorine is partially covered on one layer. On the other hand, the final product from the “para” configuration is the boat-type C₁F (Figure S5B in the Supporting Information). Thus, we think that the experimentally reported C₁F structure of boat-type^{9c} would be formed by the mechanism shown in Figure S5B in the Supporting Information.

Diffusion of fluorine on the surface of graphene is another important aspect to understand the formation mechanisms of graphite fluorides,²⁰ indicating that consideration of kinetics together with thermodynamics would be more meaningful. Thus, on the basis of the DFT results shown in this work, we are developing the reactive force field method²¹ simulating formation and dissociation of chemical bonds to address the kinetic issue, which will be reported later.

Also, it is of interest to compare patterns of graphite fluorination studied in this work with ones of carbon

- (20) Ewels, C. P.; Van Lier, G.; Charlier, J.-L.; Heggie, M. I.; Briddon, P. R. *Phys. Rev. Lett.* **2006**, *96*, 216103.
- (21) (a) van Duin, A. C. T.; Dasgupta, S.; Lorant, F.; Goddard, W. A., III. *J. Phys. Chem. A* **2001**, *105*, 9396. (b) van Duin, A. C. T.; Strachan, A.; Stewart, S.; Zhang, Q. S.; Xu, X.; Goddard, W. A., III. *J. Phys. Chem. A* **2003**, *107*, 3803. (c) Han, S. S.; van Duin, A. C. T.; Goddard, W. A., III.; Lee, H. M. *J. Phys. Chem. A* **2005**, *109*, 4575. (d) Han, S. S.; Kang, J. K.; Lee, H. M.; van Duin, A. C. T.; Goddard, W. A., III. *J. Chem. Phys.* **2005**, *123*, 114703.

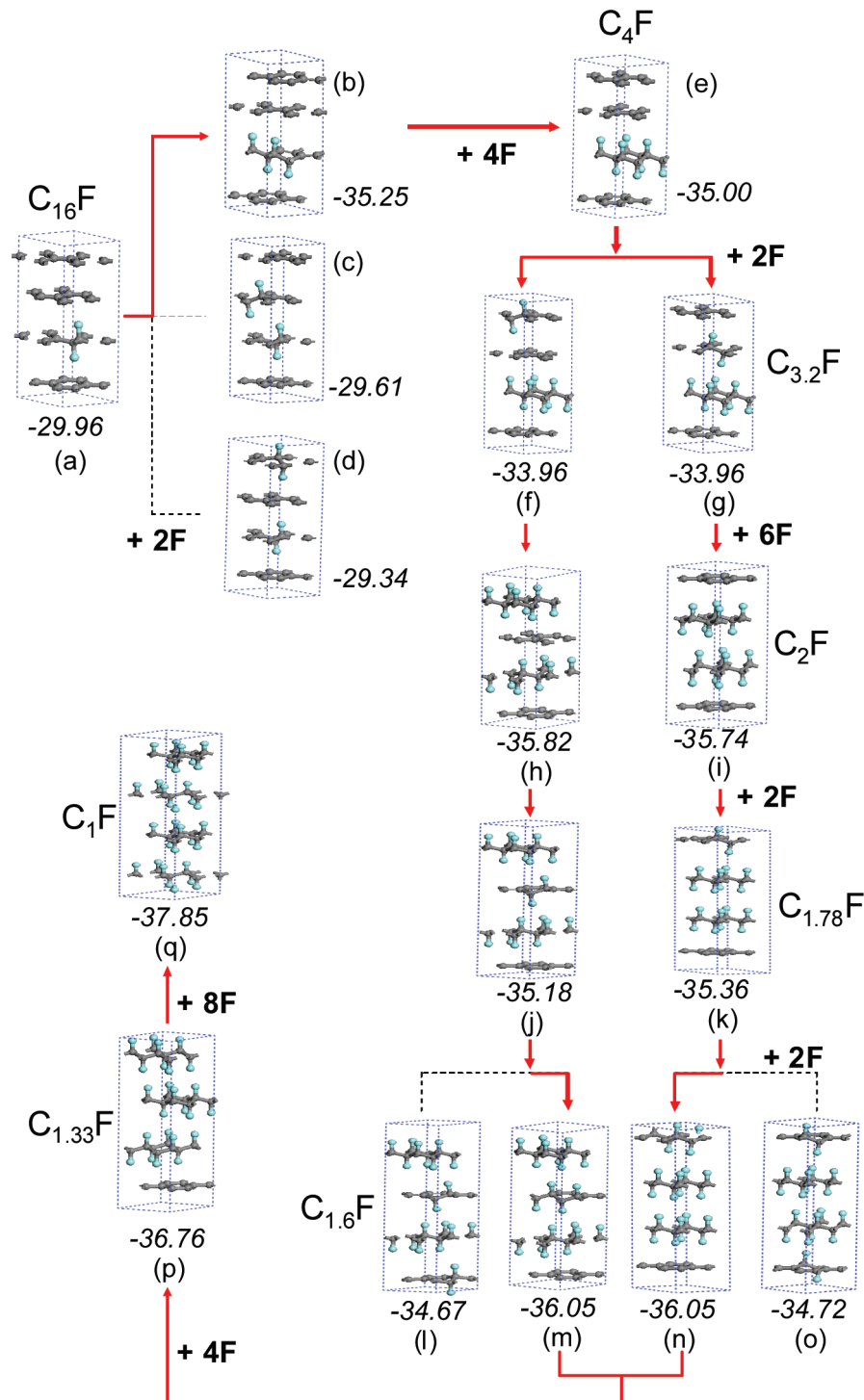


Figure 11. Formation mechanism of graphite fluorides when a fluorine source is atomic fluorine. The numbers underneath the structures indicate their heats of formation (in kcal/mol) relative to pure graphite and a F_2 molecule, calculated by DFT.

nanotube (CNT). Curvature of the tube structure makes the carbon atoms less aromatic and more reactive than a graphene layer. Thus, the binding energies of fluorine atoms on a CNT are higher than for graphite (or graphene).²⁰ Correspondingly, the curvature affects a migration barrier of fluorine atoms on the CNT surface where it modifies the ground state binding but has less of an effect on the saddle point energy, leading to higher migration barrier. Therefore, a fluorine atom diffuses more rapidly on graphene than on CNT.

The C–C bonds perpendicular to the tube axis are found to be slightly longer than the bonds parallel to the axis,²² indicating that the fluorination patterns of SWCNT would depend on chirality of the nanotube. In a case of zigzag SWCNT, the fluorination atoms were found to preferentially add next to each other in such a

(22) (a) Bettinger, H. F.; Kudin, K. N.; Scuseria, G. E. *J. Am. Chem. Soc.* **2001**, 123, 12849. (b) Kudin, K. N.; Bettinger, H. F.; Scuseria, G. E. *Phys. Rev. B* **2001**, 63, 045413.

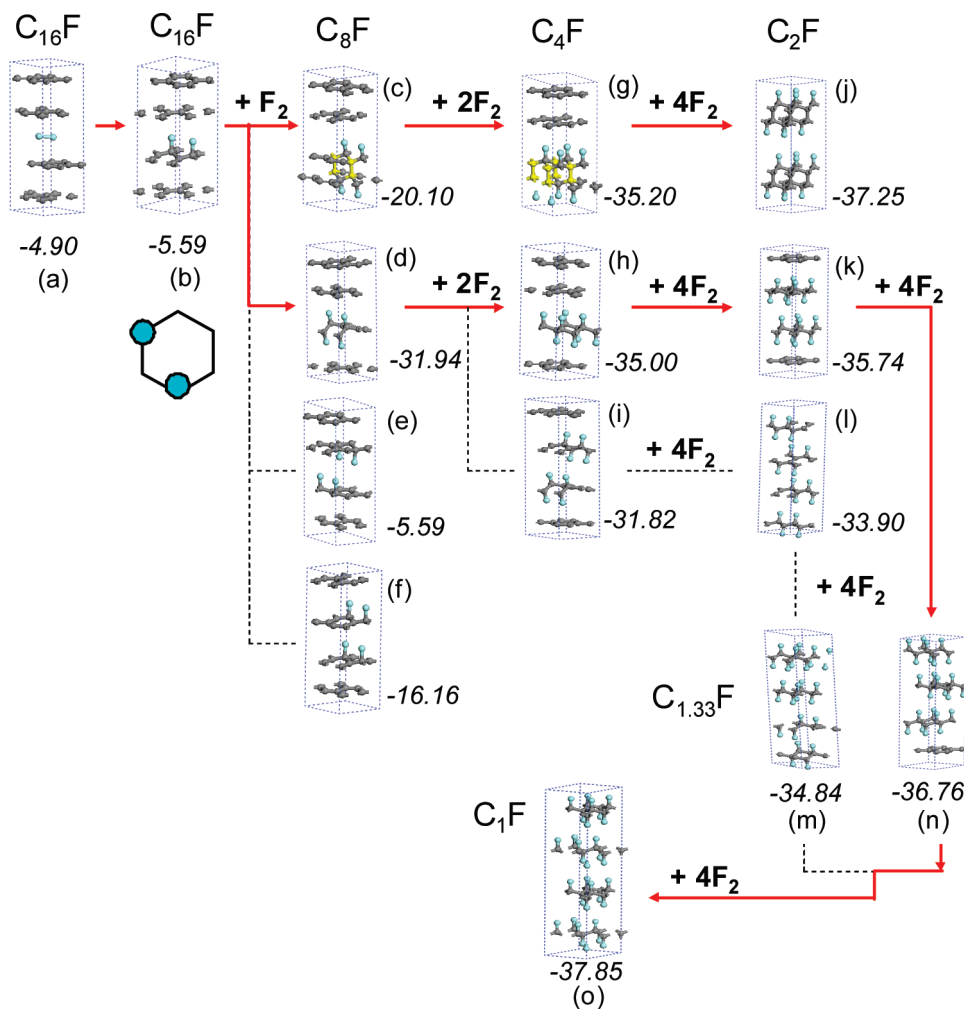


Figure 12. Formation mechanism of graphite fluorides when a fluorine source is molecular fluorine. The numbers underneath the structures indicate their heats of formation (in kcal/mol) relative to pure graphite and a F_2 molecule, calculated by DFT.

way as to form a chainlike fluorine arrangement parallel to the tube axis.^{22b} The chainlike fluorination arrangement was also observed in graphites shown in Figure 11. Moreover, similar to graphite, the fluorination on both sides of a SWCNT is thermodynamically more stable than on one side only.^{22b} Of course, the endohedral fluorination would be unfavorable in narrow CNTs. Besides, the complete fluorination (formation of C_1F) of a few outside layers of multiwalled CNTs found in an experiment²³ would occur by the mechanism (Figure 11) shown in this work.

Twelve-Layer Calculations with the Dreiding-Force Field

For this work, on the formation mechanism of graphite fluorides, we only considered crystal structures with four carbon layers due to the DFT calculation cost, which leads to two extremely ordered crystal structures for C_2F , Figure 11h,i. However, in the real experiment, more carbon layers are available; as such C_2F structures in which half the layers are fully fluorinated and the other half are pristine can have disordered crystal structures,

since the fluorinated/pristine layers can occur in any sequence. To investigate the influence of this disorder on the experimental XRD patterns, we optimized 12 C_2F crystal structures including 12 carbon layers, half pristine and half fully fluorinated, in different stacking sequences, seen in Figure 13. This optimization was performed using the Dreiding-force field.²⁴

After calculating XRD patterns of each crystal structure in Figure 13, we averaged the 12 XRDs (Figure 14) and then compared it with an experimental XRD peak (see Figure 4) of the C_2F system. The smoothed XRD pattern of Figure 14 indicates five peaks in the 2θ range of $5\text{--}90^\circ$ which are found at 8.3° , 14.5° , 28.3° , 43.0° , 60.5° , and 74.8° . These XRD patterns are similar to the experiment,⁷ which reports five peaks at 10.8° , 19.2° , 30.8° , 41.6° , and 75.0° . No peak around 60° is reported in experiment, but this peak has a low intensity in our calculated spectrum and as such may have been missing in the experiment. The first three peaks in both simulational and experimental XRDs result from $(00l)$ surfaces relating with an interlayer distance of the C_2F system, and they are found at lower angle in the current simulation

(23) Hamwi, A.; Alvergnat, H.; Bonnamy, S.; Béguin, F. *Carbon* **1997**, *35*, 723.

(24) Mayo, S. L.; Olafson, B. D.; Goddard, W. A., III. *J. Phys. Chem.* **1990**, *94*, 8897.

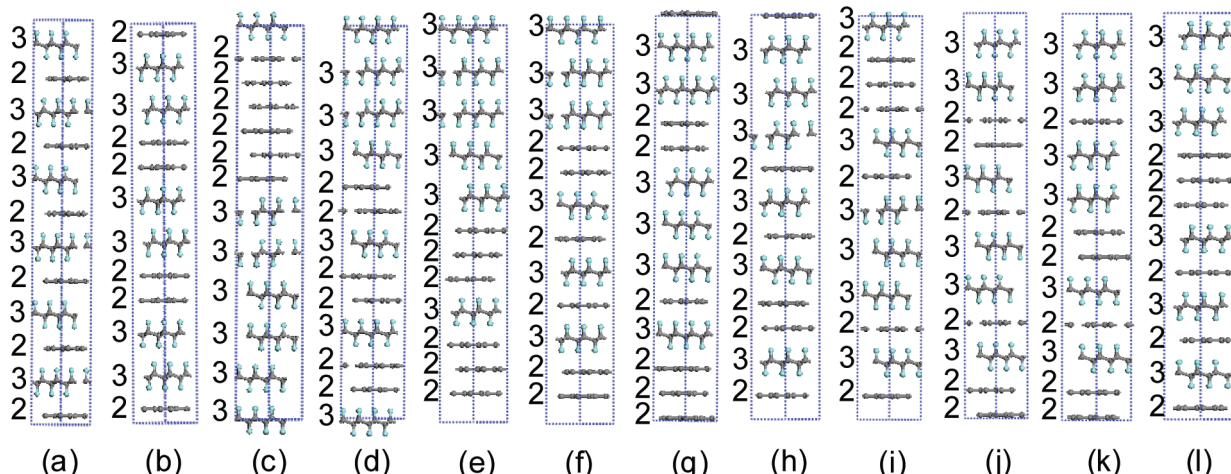


Figure 13. Twelve C_2F ($\text{CF}_{0.5}$) crystal structures with 12 carbon layers where six carbon layers have sp^2 hybridization and the rest of the carbon layers have sp^3 character. Here, the number of 2 and 3 indicate the sp^2 carbon layer and the sp^3 layer, respectively. Here, the first two crystal structures (a) and (b) are the same as the structures in Figures 11h,i, respectively.

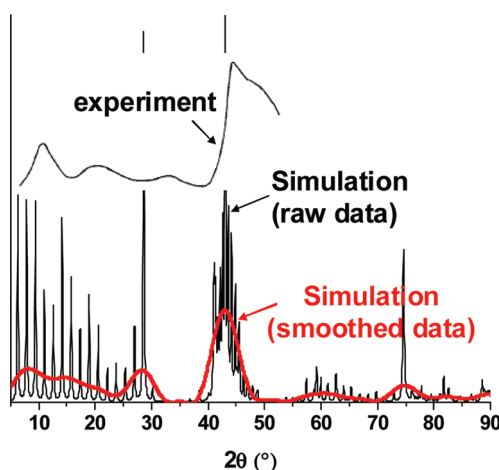


Figure 14. Simulated XRD pattern obtained by averaging XRDs of 12 C_2F ($\text{CF}_{0.5}$) structures shown in Figure 13. Here, the black and red indicate raw and smoothed (Savitzky-Golay method) data, respectively. The experimental XRD is from the reference 7.

than the experiment, indicating that the current simulation using an empirical force field slightly overestimates the interlayer distance. However, these findings reinforce our claim that the accurate C_2F crystal structural model is of a type depicted in Figure 3f, with both sp^2 and sp^3 carbon hybridization.

Summary

Using a DFT calculation, we clarified the structural model of graphite fluorides for several fluorine compositions. The most stable structure of the C_1F (CF_1) contains an infinite array of trans-linked cyclohexane chairs of covalent C–F bonds similar to the previous model experimentally proposed; however, we find that the effect of the layer stacking sequence is not significant. On the basis of our DFT-results, we propose a new C_2F ($\text{CF}_{0.5}$)

crystal structure in which half of the carbon atoms has sp^3 hybridization due to C–F covalent bonds and the other half has sp^2 hybridization as in pristine graphite. In addition, our DFT calculation proposes the formation mechanism of the graphite fluorides. Initially, two fluorines are positioned at adjacent carbon atoms with the trans geometry, followed by full fluorination of one graphene layer while other layers remain pristine. After fully covering one layer with fluorine, the next added fluorine is located on a new pristine graphene layer, until in the end all carbon layers are covered with fluorine leading to the formation of C_1F crystal. Through this mechanism, we can explain the phase transition from the C_2F to the C_1F phase, which was observed in the experiment. In addition, we find that the C_2F structure depends on a fluorine source. In other words, in the case that a fluorine source is fluorine atoms, the reported C_2F structure suggested by Touhara et al. would never be found; however, by direct fluorination of F_2 gases, the structure could be found together with our model suggested in this work.

Acknowledgment. The facilities of the Materials and Process Simulation Center were supported by ONR-DURIP and ARO-DURIP. S.S.H. was partially supported by the Hydrogen Energy R&D Center, one of the 21st Century Frontier R&D program, funded by the Ministry of Education, Science and Technology of Korea. This work was supported by MARCO/FENA (HJ and WAG). W.A.G. also acknowledges support from the WCU programs through NRF of Korea funded by the MEST (R31-2008-000-10055-0).

Supporting Information Available: The detailed information of C_2F ($\text{CF}_{0.5}$) crystal structures shown in Figure 3 and additional DFT results on the formation mechanism of graphite fluorides (PDF). This material is available free of charge via the Internet at <http://pubs.acs.org>.